This indicated the lack of osteogenic potential of *Adq*-cells in the tail. To further confirm this finding, and to rule out potential inhibitory effects of the local microenvironment, we performed heterotopic transplantation of adherent cells grown after enzymatic digestion of tail vertebrae. The cells were harvested from 2-month-old *Adq-mTmG;Gsα^{R201C}* and *Adq-mTmG* control mice, cultured in vitro (Fig. 7b) and transplanted with ceramic particles into the back of immunocompromised mice (Fig. 7c). After 8 weeks, bone tissue was detected in all samples (Fig. 7d, e). However, despite the presence of GFP-labeled adherent cells in the cell cultures (Fig. 7b) only Tomato positive osteocytes were detected by confocal analysis in all transplants (Fig. 7f, g). GFP labeling was restricted to marrow adipocytes (Fig. 7f, g) and, in *Adq-mTmG;Gsα^{R201C}* samples, to a small number of stromal cells distributed within the marrow spaces (Fig. 7g).

The expression of Gsα^{R201C} in Adq-cells is associated with cortical lysis and trabecular tunneling (dissecting) resorption

Stimulation of bone resorption was a persistent feature of *Adq-Gsα^{R201C}* mice at all ages. While in young mice it involved predominantly the bone surface in the trabecular bone (Fig. 2a, b), during mouse growth, abnormal bone resorption was also observed around some blood vessels running within the cortical bone and in the larger, predominantly sub-cortical, bone trabeculae. Consequently, areas of lysis (increased porosity) and tunneling (dissecting) resorption developed in cortical and trabecular bone respectively. This phenotype was markedly expressed in the tail vertebrae (Fig. 8a–e) in which osteoclast-enriched lytic lesions (Fig. 8c, d) tended to expand over time and were always filled by a stromal tissue that was ALP-positive/OSX-negative and expressed RANKL, as assessed by immunohistochemistry (Fig. 8e). In *Adq-mTmG;Gsα^{R201C}* mice, GFP labeling was observed in perivascular cells and in some stromal cells within lytic regions, but not in the surrounding bone cells (Fig. 8f, g). Areas of cortical and trabecular bone resorption were also observed in other skeletal segments such as long bones and lumbar vertebrae (Fig. S7a). However, at these sites, the pattern of evolution was different compared with the tail since the resorption spaces were progressively replaced by hematopoietic marrow (Fig. S7b). In *Adq-mTmG;Gsα^{R201C}* mice, GFP labeling was localized to perivascular cells at sites of lesion development and in osteoblasts bordering the lytic area (Fig. S7c, d).

DISCUSSION

Adipoq-Cre recombination in the mouse skeleton occurs in marrow adipocytes, in a network of stromal cells residing among hematopoietic cells and around blood vessels, and in cells lining the trabecular bone surfaces.[11,13–15] *Adq*-marrow stromal cells were reported to coincide with a fraction of *Lepr-Cre*-targeted stromal cells[13] and to largely overlap with the PDGFRβ^{+}/VCAM-1^{+}/CXCL12^{+} (CAR) stromal cell subsets.[14] In addition, it was shown that the majority of *Adq*-marrow stromal/perivascular cells are post-natal adipocyte progenitors, named MALPs, that support marrow vasculature and are involved in the regulation of bone resorption.[11,12] Here we show that *Adq-Cre* in bone marrow targets a population that includes stromal cells, some of which express LEPR, and perivascular cells. This *Adq-Cre*-targeted cell population is associated with an osteogenic activity that is expressed in the metaphysis of different skeletal segments in physiological conditions and in the diaphysis of long bones under specific stimulatory settings.

Adq-Cre targeting of osteoblasts was previously noted by Zhou et al. as a rare event in vivo[13] and by Mukohira et al. as an age-dependent phenomenon[14] but neither further investigated its significance. In agreement with Mukohira's report, we observed that in *Adq-mTmG* mice, GFP-labeled osteoblasts were virtually absent at a very young age, but their number progressively increased in the metaphyseal region of the long bones and lumbar vertebrae during mouse growth. This suggested the existence of *Adq*-marrow stromal osteoprogenitor cells that undergo progressive, age-dependent recruitment to trabecular bone formation and remodeling. This hypothesis was supported by the presence of GFP-positive osteoblasts and osteocytes in heterotopic ossicles made by BMSCs. Previously, other groups performed in vivo transplantation studies that failed to reveal the osteogenic potency of the *Adq*-marrow stromal compartment.[11] Although we cannot exclude *Adipoq* promoter activation during the transplantation process, the expression of osteogenic activity in our transplants, could be ascribed to the different experimental conditions used in the in vivo assays compared with previous studies. For example, while in previous work, gelatin sponges (Gelfoam^{TM}) were used as a carrier and the constructs were analyzed after 4 weeks,[11] we transplanted the cells with a ceramic carrier and harvested the ossicles after 8 weeks. Thus, it is possible that the type of carrier and the longer time before harvesting in our experiments generated the optimal conditions for *Adq*-marrow stromal progenitors to express their osteogenic potency in vivo. In addition, we did not perform cell sorting before transplantation and we cannot exclude the possibility that *Adq*-cell survival and differentiation was favored in the presence of different populations of marrow stromal cells. Based on the evidence that *Adq*-marrow stromal cells represent an adipogenically committed cell population[11,12] and that GFP-labeled adipocytes are also observed in our heterotopic ossicles, our data point to the existence of a subset of *Adq*-progenitors that are able to generate both adipocytes and osteoblasts.

The involvement of *Adq*-marrow stromal cells in both bone resorption and bone formation and the regulatory role played the Gsα/cAMP pathway in the two processes may explain the skeletal phenotype of *Adq-Gsα^{R201C}* mice. The Gsα/cAMP pathway is known to enhance the osteoclastogenic activity of marrow osteoprogenitor cells by initially stimulating the secretion of RANKL,[16–19] which is physiologically produced by *Adq*-marrow stromal cells.[12] On the other hand, Gsα is also known to stimulate cell commitment and subsequent bone formation within the osteogenic lineage.[8,20] In *Adq-Gsα^{R201C}* mice at 3 months of age, increased *Rankl* expression by mutated stromal cells leads to the prevalence of trabecular bone resorption over bone formation, in spite of the increased osteoblastogenesis. During growth of the mouse, when the *Adq*-stromal compartment expands, as demonstrated in control *Adq-mTmG* mice, the Gsα mutation massively stimulates its osteogenic differentiation. Thus, in 9-month-old mice, bone formation prevails over bone resorption, leading to a high trabecular bone mass phenotype, despite the persistent increase in *Rankl* levels.

Of note, previous work demonstrated that in the bone marrow stromal compartment, Gsα enhances osteogenic differentiation at the expense of adipogenesis;[21,22] accordingly, in *Adq-Gsα^{R201C}* mice, bone formation is associated with an overall reduction in bone marrow adipose tissue. We did not investigate the phenotypic effects and functional mechanisms affected by *Gsα^{R201C}* in *Adq*-marrow stromal cells. However, we showed that the events observed in *Adq-Gsα^{R201C}* mice were reproduced in heterotopic transplants in which the presence of *Adq-Gsα^{R201C}* marrow stromal cells associated with an unusual extensive "resorption"/disintegration of the ceramic particles[23] and with the deposition of a high amount of bone that was largely made by GFP-positive bone cells.

Interestingly, our *Adq-Gsα^{R201C}* transgenic model also demonstrated that a synergy exists between Gsα^{R201C} and estrogen in stimulating bone formation by *Adq*-stromal cells within the diaphyseal marrow of long bones. The role of estrogen in this ectopic and non-structural osteogenic process was suggested by its spontaneous appearance in *Adq-Gsα^{R201C}* female mice and was confirmed by its reproduction in male mice treated with

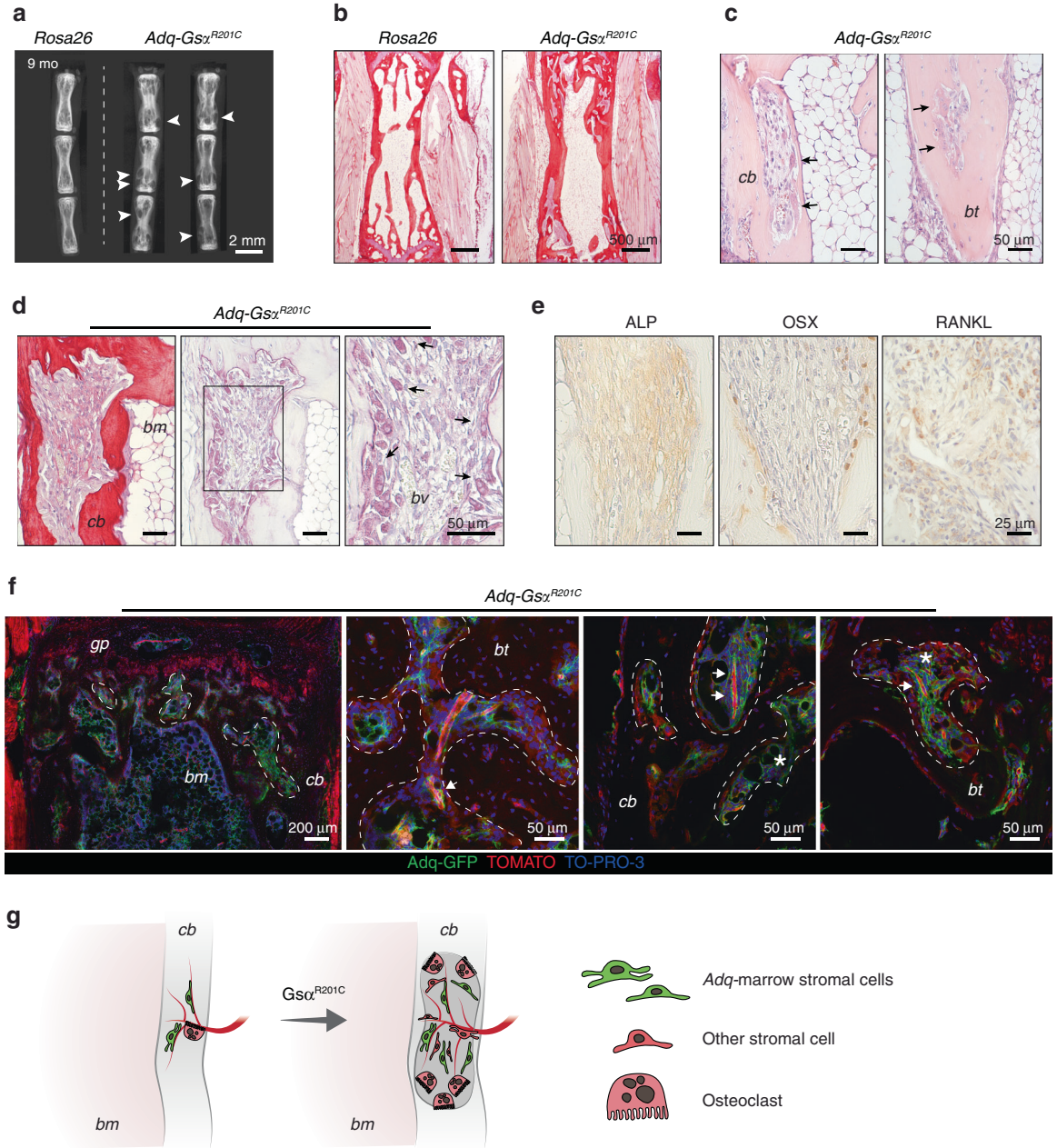

Fig. 8 *Adq*-intraosseous pericytes associate with lytic lesions in cortical and trabecular bone in *Adq-Gsα^{R201C}* mice. **a** Radiographic analysis of dissected tail vertebrae from 9-month-old *Rosa26* and *Adq-Gsα^{R201C}* mice showing several osteolytic lesions (*arrowhead*). **b** Representative Sirius red stained sections of tail vertebrae from 9-month-old mice. **c** H&E-stained sections showing dissecting and tunneling resorption in tail vertebrae. Note the massive presence of osteoclasts (*black arrow*). **d** Sirius red and TRAP-stained sections showing intracortical bone resorption in tail vertebrae. Resorption areas progressed over time and were enriched in osteoclasts (*black arrow*) in close association with blood vessels (*bv*). **e** Immunolocalization of ALP, OSX and RANKL in a tail vertebra lytic lesion of *Adq-Gsα^{R201C}* mice. **f** Representative confocal images from *Adq-mTmG;Gsα^{R201C}* mice tail vertebrae showing areas of osteolysis (*dashed line*) filled with GFP-positive perivascular cells (*arrow*) and stromal cells (*asterisk*). **g** Schematic representation of lytic lesions associated with intracortical Gsα-mutated *Adq*-pericytes. *cb*: cortical bone, *bt*: bone trabecula, *bm:* bone marrow, *gp*: growth plate

exogenous hormone. Estrogen-dependent bone deposition in the marrow diaphysis is a long-known phenomenon in birds, as a physiological calcium storage mechanism during the egg-laying cycle,[24] and in female mice, as a non-physiological phenomenon induced by treatment with high doses of exogenous hormone.[25,26] However, estrogen-related medullary osteogenic processes previously reported in birds and mice relied on the activation of cells lining the endosteal surface and resulted in a centripetal process of "endosteal trabecularization".[25] In our *Adq-Gsα^{R201C}* female mice and estrogen-treated male mice, the intra-medullary bone resulted from the activation of *Adq*-stromal cells on the blood vessel abluminal side and involved the cortical endosteum only focally, consistent with the discontinuous distribution of *Adq*-cells at this site. Thus, the topographic pattern of estrogen-dependent bone formation in the diaphyseal cavity of Gsα^{R201C} mice was rather reminiscent of that observed in some estrogen-independent experimental models of medullary osteogenesis, as for example, in colchicine treated rats.[27,28] The reason why *Adq*-diaphyseal perivascular marrow stromal cells require both *Gsα^{R201C}* and estrogen to express their osteogenic potential remains to be

addressed. However, it is interesting to note that recently, Sivaraj et al. demonstrated that diaphyseal stromal progenitors have different biological properties compared with their metaphyseal counterparts including a higher baseline commitment to adipogenesis.[29] This finding may explain the different response of metaphyseal and diaphyseal *Adq*-marrow stromal cells to *Gsα*^{R201C} in our *Adq-Gsα*^{R201C} transgenic model. In metaphyseal *Adq*-marrow stromal cells, *Gsα*^{R201C} alone was sufficient to stimulate the osteogenic function that was further enhanced by estrogen. In contrast, in diaphyseal *Adq*-marrow stromal cells the synergic action of both stimuli was required to trigger and complete the osteogenic program.

Regardless of the mechanism of synergy of Gsα^{R201C}and estrogen to enhance osteogenesis, the marrow osteogenic process in *Gsα*^{R201C} mice provides further in situ evidence of the ability of *Adq*-marrow stromal cells to form bone and has some interesting implications. First, it reveals that R201-mutated *Gsα* and estrogen together may induce an osteogenic fate choice in a subset of *Adq*-stromal cells that do not form bone in physiological conditions. Further investigation of this phenomenon may help to better understand the process of osteogenesis and to therapeutically approach low bone mass diseases. Second, consistent with Sivaraj's work,[29] it shows for the first time and in the intact bone, there is a major difference in the regulation of diaphyseal *Adq-Cre*-targeted osteoprogenitor cells compared with their metaphyseal counterparts and it seems to confirm the existence of an "internal plasticity"[29] in the marrow stromal cell system. Finally, our data show that *Adq-Gsα*^{R201C} mice provide a unique model to study bone formation by marrow diaphyseal stromal cells in mammals in the absence of any type of mechanical or pharmacological manipulation of the local microenvironment and/or of hematopoiesis.

Interestingly, the metaphyseal and diaphyseal osteogenic activities of *Adq*-cells were not homogeneously distributed throughout the mouse skeleton since neither calvaria nor the tail vertebrae ever showed *Adq-Cre*- targeted osteoblasts and osteocytes. The reason for the lack of osteogenic activity of *Adq*-cells at these skeletal sites remains to be clarified. Meanwhile, we ruled out potential inhibitory effects of the local microenvironment by demonstrating that marrow stromal cells isolated from the tail of *Adq-mTmG;Gsα*^{R201C} mice did not form GFP-labeled bone cells in heterotopic transplants.

In this work, we also identified a compartment of *Adq*-perivascular cells within the cortical bone that was unnoticed in previous studies. Consistent with this finding and with the evidence that *Gsα*^{R201C} enhances the bone resorption stimulatory activity of *Adq*-marrow stromal cells, as shown in this study, *Adq-Gsα*^{R201C} mice developed a cortical lytic (increased porosity) and trabecular tunneling (dissecting) resorption phenotype that was particularly evident in the tail vertebrae. This phenotype may indicate a role for *Adq*-perivascular cells in the physiological remodeling of the transcortical vascular channels.[30] In addition, it may shed some light on the cell type involved in the pathogenesis of Gsα-related skeletal diseases with abnormal bone resorption such as hyperparathyroidism and certain phases of lesion development in FD of bone.

FD is a severely crippling skeletal disorder associated with Gsα activating mutations.[5] In FD lesions, normal bone is resorbed and replaced by fibrous marrow and newly formed, woven bone. We previously reported a FD phenotype in transgenic mice with ubiquitous expression of the *Gsα*^{R201C} mutation.[7] Our current study shows that specific aspects of the FD phenotype are also reproduced in *Adq-Gsα*^{R201C} mice, thus revealing the involvement of the *Adq*-marrow stromal cell subset in the pathogenesis of the disease. Specifically, it suggests that Gsα-mutated *Adq*-marrow stromal cells might act as the trigger of the bone resorption processes (cortical lysis and dissecting resorption) that precedes the growth of the fibro-osseous tissue, and that they might also contribute to the deposition of FD bone. Interestingly, the post-natal appearance and progressive expansion of the *Adq*-marrow stromal cell network perfectly fit with the natural history of this skeletal dysplasia that, despite the early post-zygotic occurrence of the Gsα mutation, does not affect embryonic and fetal development of the skeleton, appears after birth, and worsens during skeletal growth.[31] Thus, although *Adq-Gsα*^{R201C} mice fail to develop the full-blown FD skeletal phenotype observed in mice with ubiquitous and constitutive expression of *Gsα*^{R201C} [7], they could represent a useful tool to study the early stages of FD lesion development.

CONCLUSION

In conclusion, in this work we demonstrated that *Adq*-cells in the marrow stromal cell network act not only as stimulators of bone resorption, but also as osteoprogenitor cells. We also showed that Gsα mediates their regulatory and progenitor functions and that the activity of the Gsα/cAMP signaling pathway must be tightly controlled in the entire *Adq*-marrow cell network in order to preserve the homeostasis of the post-natal bone/bone marrow organ.

MATERIALS AND METHODS

Mice generation

All studies were performed in compliance with relevant Italian laws and Institutional guidelines and all procedures were IACUC approved.

To generate the *Rosa26-lsl-*Gsα^{R201C} vector, the SalI/HindIII cassette was excised from the *R201C* rat *Gsα* cDNA, which included a hemagglutinin (HA) epitope as a flag (ATCC 63317, GenBank M12673),[32] and inserted it into the pBigT vector (Addgene #21270), which contained a splicing acceptor site of adenovirus (SA), a stop region, including a neo cassette downstream to the PGK promoter and, downstream, a triple SV40 polyadenylation sequence. The stop cassette was flanked by two *loxP* sites and followed by the bovine growth hormone polyadenylation signal (BGHpA). The PacI and AscI restriction sites, placed 5′ to the SA and 3′ to the BGHpA, respectively, were used to subclone the functional sequence into the pRosa26PA plasmid (Addgene #21271), which included the *Rosa26* sequences required for targeted recombination into the murine *Rosa26* locus. *R26-lsl-Gsα*^{R201C} mice were generated by electroporating the *R26-lsl-*Gsα^{R201C} vector into murine ES CK35 (129/Sv Pas strain) cells. Upon electroporation, mouse ES cells were selected by neo screening, and 216 neo resistant clones were analyzed by multiple PCRs and sequencing. Two positive ES clones were implanted in C57Bl/6 N blastocysts, which, in turn were transferred into surrogate B6CBAF1 female mice. Mouse chimeras were backcrossed with C57Bl/6 N and F1 animals were genotyped by PCR. Heterozygous F1 mice were obtained from both founder clones. Two lines were serially backcrossed and showed regular Mendelian inheritance of the transgenic cassette.

Homozygous (homo) *R26-lsl-Gsα*^{R201C} mice (*Rosa26*) were crossed with heterozygous (het) *Adipoq-Cre* mice (#028020, The Jackson Laboratory); the resulting progeny were crossed again with Rosa26 mice to generate *Adiponectin-Cre*(het);*R26-lsl-Gsα*^{R201C}*(*homo) (*Adq-Gsα*^{R201C}) mice, which expressed the mutant form of *Gsα* in adipogenic cells.

To generate *Adq-mTmG* and *Adq-mTmG;Gsα*^{R201C} lineage reporter mice, we crossed heterozygous *Adq-Cre* and double heterozygous *Adq-Gsα*^{R201C} mice with homozygous *loxP-mT-pA-loxP-mG-pA* (*mTmG*) mice (#007676 The Jackson Laboratory). The triple heterozygous *Adq-mTmG;Gsα*^{R201C} mice harbor one R26 allele with *Gsα*^{R201C} transgene while the other *R26* allele contains the *mTmG* transgene.

All mice were maintained in cabin-type isolators at standard environmental conditions (temperature 22–25 °C, humidity 40%–70%) with 12:12 h dark/light photoperiod. Food and water

Table 1. Sequence of primers used for genotyping and qPCR

Genotyping	
Mouse strain	**Sequence 5′ − 3'**
Adipoq-Cre	F: GCATTGCTGTCACTTGGTCGT
	R: CGATGCAACGAGTGATGAGG
R26-lsl-Gsα^{R201C}	F: AAAGTCGCTCTGAGTTGTTAT
	R: GCGAAGAGTTTGTCCTCAACC
	R: GGAGCGGGAGAAATGGATATG
R26-mTmG	F: CTCTGCTGCCTCCTGGCTTCT
	R: CGAGGCGGATCACAAGCAATA
	R: TCAATGGGCGGGGGTCGTT
qPCR	
Gene	**Sequence 5′ − 3'**
Alpl	F: CCAGAAAGACACCTTGACTGTGG
	R: TCTTGTCCGTGTCGCTCACCAT
Bglap	F: GCAATAAGGTAGTGAACAGACTCC
	R: CCATAGATGCGTTTGTAGGCGG
Col1a1	F: CAGGGTATTGCTGGACAACG
	R: TTGTTTGCCAGGTTCACCAGA
Gapdh	F: CATCACTGCCACCCAGAAGACTG
	R: ATGCCAGTGAGCTTCCCGTTCAG
HA (R26-Gnas)	F: GAAGAGGACGTGCCGGATTAC
	R: TGGTTTCAATGGCCTCCTTCA
Opg	F: CGGAAACAGAGAAGCCACGCAA
	R: CTGTCCACCAAAACACTCAGCC
Rank	F: GGACAACGGAATCAGATGTGGTC
	R: CCACAGAGATGAAGAGGAGCAG
Rankl	F: CGAGCGCAGATGGATCCTAA
	R: GCAGGAGTCAGGTAGTGTGT
Runx2	F: CCTGAACTCTGCACCAAGTCCT
	R: TCATCTGGCTCAGATAGGAGGG
Sp7	F: GGCTTTTCTGCGGCAAGAGGTT
	R: CGCTGATGTTTGCTCAAGTGGTC

were provided *ad libitum*. Mice were genotyped by using the oligonucleotides listed in Table 1.

X-ray analysis and micro-CT scanning

Radiographic analyses were performed on femora and tibiae using Faxitron MX-20 Specimen Radiography System (Faxitron X-ray Corp., Wheeling, IL, USA) set at 24–25 kV for 6–8 s with Kodak MIN-R2000 18 × 24 films.

For micro-CT scanning, tibiae were placed within a plastic tube, mounted onto the instrument rotational stage and scanned at 8 µm voxel size using 80 kV, 50 µA X-ray settings and a 1 mm aluminum filter with exposure time of 100 ms per frame, with a Bruker SkyScan 1275 micro-CT (Micro Photonic, Allentown, PA, USA). Three-dimensional reconstruction was performed with Bruker's NRecon software and visualization occurred using Bruker's DataViewer and CTscan software programs.

Histology

Mice were euthanized by carbon dioxide inhalation and skeletal segments were dissected and processed for either paraffin embedding, methylmethacrylate (MMA) or gelatin embedding.

For paraffin embedding, samples were fixed with 4% formaldehyde in PBS pH 7.4 for 48 h at 4 °C and decalcified in 10% EDTA for 14–21 days at 4 °C with gentle shaking. Three-micron-thick sections were used for standard histology after staining with Hematoxylin-Eosin (H&E) or with Sirius red to visualize collagen fibers, for Tartrate-Resistant-Acid-Phosphatase (TRAP) histochemistry to highlight cells of the osteoclastic lineage and for histomorphometry.

MMA embedding was performed on undecalcified bone segments. After dissection, bone samples were fixed in 4% formaldehyde for 24 h and dehydrated through a series of increasing ethanol concentrations. Bones were then infiltrated for 3 days with the plastic embedding mixture containing 60 mL of MMA, 35 mL butylmethacrylate, 5 mL methylbenzoate, 1,2 mL polyethylene glycol 400 and 0.8 g of dry benzoyl peroxide. The polymerization mixture was prepared by adding 400 µL of N,N-dimethyl-p-toluidine to the infiltrating solution. Sections of 4–7 µm in thickness were cut from MMA blocks, deplasticized with 2-methoxyethylacetate (all reagents were purchased from Sigma Aldrich, Saint Louis, MO, USA), stained with Von Kossa and counterstained with Van Gieson.

For gelatin embedding, freshly dissected femora, tibiae and tail vertebrae were fixed in cold 4% formaldehyde solution for 4 h, washed in 1X PBS and decalcified in 0.5 M EDTA at 4 °C. Soft tissues were fixed in 4% formaldehyde for 4 h. Samples were then placed in 20% sucrose and 2% Polyvinylpyrrolidone (PVP) solution in PBS for a further 48 h. Samples were embedded in an 8% porcine gelatin solution containing 20% sucrose and 2% PVP as previously reported.[33] Twenty to 50 µm-thick sections were cut, air-dried for 30 min, hydrated with 1X PBS, stained with TO-PRO-3 (#T3605, Thermo Fisher Scientific, Waltham, Massachusetts, USA) for nuclei visualization and imaged with Leica Confocal Microscope (Wetzlar, Germany). For heterotopic transplants, gelatin embedded samples were also used to perform TRAP and Alkaline Phosphatase (ALP) histochemistry.

For measurements of GFP-positive BMSC area (*Adq*-GFP^{+} BMSC Ar/Ma.Ar), pictures at 40X magnification were taken with Leica Confocal Microscope, color channel split by ImageJ software and green channel used for quantification of the area of signal that was then normalized on the marrow area. The fraction of GFP-labeled osteocytes (GFP^{+} osteocytes) was calculated by counting them on bone trabeculae of femora and tibiae.

Histochemistry

TRAP and ALP histochemistry were performed using Sigma Aldrich reagents (Sigma Aldrich). Briefly, for TRAP histochemistry working solution, 50 mg of Naphtol AS-BI phosphate were dissolved in 4 mL N,N-dimethylformamide added to 4 mL acetate buffer and 92 mL of distilled water; then, 150 mg of Tartaric Acid and 30 mg of Fast Garnet were added. The slides were incubated with the working solution at 37 °C. For histochemical detection of ALP on gelatin sections, 30 mg of Naphtol AS Phosphate were dissolved in 0,5 mL N,N-dimethylformamide and added to a 100 mL borate buffer with 100 mg of AS blue BB salt. The solution was added to the slide and incubated for 5–10 min at 37 °C.

Immunohistochemistry

Immunolocalization of OSX, RANKL and ALP was performed using rabbit anti-mouse antibodies (anti-OSX #ab22552, anti-RANKL #ab37415, Abcam, Cambridge, UK; anti-ALP # 11187–1-AP, Proteintech, Rosemont, Illinois, USA) applied at a dilution of 1:200 in PBS + 1% turn BSA, overnight at 4 °C. After repeated washing with PBS, sections were incubated for 30 min with biotin-conjugated swine anti-rabbit IgG (#P0217, Agilent, Santa Clara, CA, USA) 1:200 in PBS + 1% BSA and then exposed for 30 min to peroxidase-conjugated ExtrAvidin (#P0217, Agilent) (1:50 in PBS + 1% BSA). The peroxidase reaction was developed using DAB substrate kit (SK-4100, Vector Laboratories, Burlingame, CA, USA).

Immunolocalization of LEPR, endomucin (EMCN) and alpha-smooth muscle actin (α-SMA) was performed using goat anti-LEPR (#AF497, R&D Systems, Minneapolis, MN, USA), rat anti-EMCN (#ab106100, Abcam) and rabbit anti-α-SMA (#ab5694, Abcam).

Twenty-five µm-thick sections from gelatin-embedded samples were rehydrated with PBS and then immunostained overnight. After primary antibody incubation, sections were repeatedly washed with PBS and incubated with appropriate Alexa Fluor 647-conjugated (rabbit anti-goat IgG #A-21446, goat anti-rat IgG #A-21247, goat anti-rabbit IgG #A27040 Thermo Fisher Scientific) secondary antibodies for 1 h at room temperature. Nuclei were counterstained with TO-PRO3.

Histomorphometry

Quantitative bone histomorphometry was conducted on lumbar vertebrae (3rd and 4th) and on distal femora. Experiments were performed in a blinded fashion. Different bone parameters, using standard nomenclature and abbreviations,[34] were measured in a region of interest (ROI) in the secondary spongiosa of distal femora, starting 300 µm below the growth plate and for a length of 1 mm, and between the two growth plates in lumbar vertebrae. H&E and Sirius red-stained sections were used to measure trabecular bone volume per tissue volume (BV/TV), osteoblast number per bone surface (N.Ob/BS) and osteoblast surface per bone surface (Ob.S/BS). TRAP-stained sections were used to measure osteoclast number per bone surface (N.Oc/BS) and osteoclast surface per bone surface (Oc.S/BS).

Dynamic bone histomorphometry was performed on lumbar vertebrae dissected from mice that were treated with 30 mg/kg of calcein (Sigma Aldrich), 5 and 2 days before euthanasia. Calcein fluorescent labeling was used to quantify mineralizing surface (MS/BS), mineral apposition rate (MAR) and bone formation rate (BFR/BS).

Bone marrow adiposity was analyzed by manual counting of the number of adipocytes per marrow area (N.Ad/Ma.Ar) and by measuring their area (Ad.Ar/Ma.Ar) in H&E-stained sections of distal femora, according to standard procedures and nomenclature.[35,36]

Pictures were acquired with an optical microscope (Zeiss Axiophot, Jena, Germany) through a digital camera (Jenoptik ProgrRes C5, Jena, Germany) and all histomorphometric analyses were performed using ImageJ.[37]

Transplantation assay

BMSCs were isolated from 3-month-old female *Adq-mTmG* and *Adq- mTmG;Gsα*^{R201C} mice by flushing long bones (femora, tibiae, humeri) and crushing sacral and lumbar vertebrae. Cell suspensions were collected after vigorous pipetting, filtered through a 70 µm nylon mesh cell strainer, and grown at 37 °C 5% CO_2 as multiclonal cell strains[38] in αMEM Sigma Aldrich) supplemented with 20% Fetal bovine serum (Thermo Fisher Scientific), 1% L-glutamine, 1% penicillin/streptomycin Sigma Aldrich). To isolate BMSCs from the tail vertebrae, the tails were skinned, cleaned of muscle and tendons and incubated in 5 mL of 2 mg·mL^{-1} Collagenase I solution in HBSS for 15 min and then spun at 200 *g* (relative centrifugal force) to remove the periosteum. The vertebrae were then minced and incubated in 10 mL of 2 mg·mL^{-1} Collagenase solution in HBSS for 1 h and spun at 100 *g*. After digestion, the supernatant was collected, filtered through 70 µm nylon mesh and centrifuged at 1 300 *g* for 6 min. The resulting pellet was washed with αMEM and cells were grown in the supplemented culture medium reported above.

After 1 week, all cell populations were transplanted. Constructs were made by loading 7×10^6 cells onto 40 mg of ceramic particles (a component of AttraX, NuVasive, San Diego, CA, USA) and transplanted into 2-month-old female CB17.Cg-Prkd^{scid} Lyst$^{bg\text{-}j}$/Crl (SCID/beige) mice (Charles River, Wilmington, Massachusetts USA) as previously described.[39] After 8 weeks, samples were harvested, fixed in 4% formaldehyde in PBS pH 7.4 for 12 h and decalcified in 0.5 mol·L^{-1} EDTA for 1 week. Samples were then processed for porcine gel embedding as described above. Ten-micron-thick sections were stained with H&E for morphology evaluation and histomorphometric quantification of the different tissue area, and for TRAP and ALP histochemistry. Twenty µm-thick sections were cut and analyzed by confocal microscopy for visualization of GFP and tdTomato fluorescence.

Estradiol treatment

For 17β-estradiol (E2, Sigma Aldrich) treatment, two experimental groups were established: a vehicle group including *Rosa26*, *Adq-Gsα*^{R201C} and *Adq-mTmG;Gsα*^{R201C} mice ($n \geq 4$ for each genotype, 5 months of age) and a E2 group including *Rosa26*, *Adq-Gsα*^{R201C} mice, *Adq-mTmG;Gsα*^{R201C} mice ($n \geq 4$ for each genotype, 5 months of age). E2 was dissolved in ethanol at a concentration of 5 mg·mL^{-1} and added to 300 mL of drinking water to a final concentration of 4 µg·mL^{-1}. The vehicle group received ethanol in drinking water at a final concentration of 0.1%. Water bottles were changed every week. The dose of E2 ingested was calculated as previously reported.[40] After 6 weeks of treatment, mice were sacrificed by CO_2 inhalation. Radiographic analyses were performed before the treatment and at sacrifice.

Gene expression analysis by quantitative PCR

Femora and tibiae from 3- and 9-month-old female mice were dissected and snap frozen in liquid nitrogen and kept at −80° until use. Bone samples were homogenized by Mikro-Dismembrator U (Gottingen, Germany) and total RNA was isolated using the TRI Reagent® (Thermo Fisher Scientific) protocol. Reverse transcription was performed by using QuantiTect® Reverse Transcription Kit (Qiagen, Hilden, Germany). cDNA samples were used as templates for quantitative PCR (qPCR) analysis on a 7500 Fast Real-Time PCR System (Applied Biosystem, Waltham, Massachusetts, USA), performed using PowerUP Sybr Green (Thermo Fisher Scientific) and specific primers (Table 1). Gene expression levels of each gene were normalized to GAPDH expression.

Statistical analysis

The comparisons between two groups were performed using the unpaired t-test. Changes in the GFP^{+} osteocyte fraction and *Adq*-GFP^{+} BMSC Area between *Adq-mTmG* and *Adq-mTmG;Gsα*^{R201C} mice at different ages were analyzed with the two-way ANOVA followed by a Sidak's multiple comparison test. The comparison of histomorphometrical parameters during estrogen treatment was performed using one-way ANOVA followed by a Tukey's multiple comparison test. In all experiments a *P*-value less than 0.05 was considered statistically significant. All graphs and statistical analyses were performed using GraphPad Prism version 8 (GraphPad Software, La Jolla, CA, USA).

DATA AVAILABILITY

The authors declare that all data supporting the findings of this study are available within the paper and its supplementary information files.

ACKNOWLEDGEMENTS

This study was supported by grants from Telethon GGP15198, University of Pennsylvania Orphan Disease Center in partnership with the Fibrous Dysplasia Foundation MDBR16-114-FD, MDBR17-114-FD, MDBR18-114-FD/MAS and Sapienza University RM11916B839074A8 to M.R.; Fibrous Dysplasia Foundation MDBR-22-101-FDMAS to B.P. and M.R.; Sapienza University RM118164289636F0 to A.C.; ZIA DE000380 to PGR; AIRC IG-24614 to I.S.

AUTHOR CONTRIBUTIONS

B.P. and M.R. designed the research study and drafted the manuscript. B.P. conducted all the experiments, acquired, analyzed the data, and oversaw all aspects of the study. R.L. is listed as co-first author as she contributed to the design of the study, conducted the experiments and acquired the data. S.D., C.R., E.S., I.C., G.F., and M.D.S.V. conducted the experiments and acquired histological and molecular data. I.S. contributed to the vector generation. MS contributed to the micro-CT analysis. P.G.R. and A.C. provided expertise related to the experiments and contributed to the

interpretation of the results. B.P., P.G.R., A.C. and M.R. edited and revised the manuscript. All the authors read and approved the manuscript.

ADDITIONAL INFORMATION

Supplementary information The online version contains supplementary material available at https://doi.org/10.1038/s41413-022-00220-1.

Competing interests: The authors declare no competing interests.

REFERENCES

1. Weinstein, L. S., Yu, S., Warner, D. R. & Liu, J. Endocrine manifestations of stimulatory G protein α-subunit mutations and the role of genomic imprinting. *Endocr. Rev.* **22**, 675–705 (2001).
2. Donsante, S. et al. From stem cells to bone-forming cells. *Int. J. Mol. Sci.* **22**, 3989 (2021).
3. Sakamoto, A. et al. Deficiency of the G-protein α-Subunit Gsα in osteoblasts leads to differential effects on trabecular and cortical bone. *J. Biol. Chem.* **280**, 21369–21375 (2005).
4. Cong, Q., Xu, R. & Yang, Y. Gαs signaling in skeletal development, homeostasis and diseases. in. *Curr. Top. Dev. Biol.* **133**, 281–307 (2019).
5. Weinstein, L. S. et al. Activating mutations of the stimulatory G protein in the McCune–Albright syndrome. *N. Engl. J. Med.* **325**, 1688–1695 (1991).
6. Collins, M. T., Boyce, A. M. & Riminucci, M. Fibrous Dysplasia. in *Primer on the Metabolic Bone Diseases and Disorders of Mineral Metabolism* (Wiley, 2018). https://doi.org/10.1002/9781119266594.ch108.
7. Saggio, I. et al. Constitutive expression of Gsα ^{R201C} in mice produces a heritable, direct replica of human fibrous dysplasia bone pathology and demonstrates its natural history. *J. Bone Miner. Res.* **29**, 2357–2368 (2014).
8. Remoli, C. et al. Osteoblast-specific expression of the Fibrous Dysplasia (FD)-causing mutation *Gsα ^{R201C}* produces a high bone mass phenotype but does not reproduce FD in the mouse. *J. Bone Miner. Res.* **30**, 1030–1043 (2015).
9. Lung, H., Hsiao, E. C. & Wentworth, K. L. Advances in models of fibrous dysplasia/McCune-Albright syndrome. *Front. Endocrinol. (Lausanne)* **10**, 925 (2020).
10. Baccin, C. et al. Combined single-cell and spatial transcriptomics reveal the molecular, cellular and spatial bone marrow niche organization. *Nat. Cell Biol.* **22**, 33–48 (2020).
11. Zhong, L. et al. Single cell transcriptomics identifies a unique adipose lineage cell population that regulates bone marrow environment. *Elife* **9**, e54695 (2020).
12. Yu, W. et al. Bone marrow adipogenic lineage precursors promote osteoclastogenesis in bone remodeling and pathologic bone loss. *J. Clin. Invest* **131**, e140214 (2021).
13. Zhou, B. O. et al. Bone marrow adipocytes promote the regeneration of stem cells and haematopoiesis by secreting SCF. *Nat. Cell Biol.* **19**, 891–903 (2017).
14. Mukohira, H. et al. Mesenchymal stromal cells in bone marrow express adiponectin and are efficiently targeted by an adiponectin promoter-driven Cre transgene. *Int. Immunol.* **31**, 729–742 (2019).
15. Zhang, X. et al. A bone-specific adipogenesis pathway in fat-free mice defines key origins and adaptations of bone marrow adipocytes with age and disease. *Elife* **10**, e66275 (2021).
16. Palmisano, B. et al. RANKL inhibition in fibrous dysplasia of bone: A preclinical study in a mouse model of the human disease. *J. Bone Miner. Res.* **34**, 2171–2182 (2019).
17. de Castro, L. F. et al. Activation of RANK/RANKL/OPG pathway is involved in the pathophysiology of fibrous dysplasia and associated with disease burden. *J. Bone Miner. Res.* **34**, 290–294 (2019).
18. Corsi, A. et al. Zoledronic acid in a mouse model of human fibrous dysplasia: Ineffectiveness on tissue pathology, formation of "Giant Osteoclasts" and pathogenetic Implications. *Calcif. Tissue Int.* **107**, 603–610 (2020).
19. Raimondo, D. et al. Changes in gene expression in human skeletal stem cells transduced with constitutively active Gsα correlates with hallmark histopathological changes seen in fibrous dysplastic bone. *PLoS One* **15**, e0227279 (2020).
20. Wu, J. Y. et al. Gsα enhances commitment of mesenchymal progenitors to the osteoblast lineage but restrains osteoblast differentiation in mice. *J. Clin. Invest.* **121**, 3492–3504 (2011).
21. Sinha, P. et al. Loss of G $_{s}$ α early in the osteoblast lineage favors adipogenic differentiation of mesenchymal progenitors and committed osteoblast precursors. *J. Bone Miner. Res.* **29**, 2414–2426 (2014).
22. Kao, R., Lu, W., Louie, A. & Nissenson, R. Cyclic AMP signaling in bone marrow stromal cells has reciprocal effects on the ability of mesenchymal stem cells to differentiate into mature osteoblasts versus mature adipocytes. *Endocrine* **42**, 622–636 (2012).
23. Boyde, A., Corsi, A., Quarto, R., Cancedda, R. & Bianco, P. Osteoconduction in large macroporous hydroxyapatite ceramic implants: evidence for a complementary integration and disintegration mechanism. *Bone* **24**, 579–589 (1999).
24. Kyes, P. & Potter, T. S. Physiological marrow ossification in female pigeons. *Anat. Rec.* **60**, 377–379 (1934).
25. Liu, C.-C. & Howard, G. A. Bone-cell changes in estrogen-induced bone-mass increase in mice: Dissociation of osteoclasts from bone surfaces. *Anat. Rec.* **229**, 240–250 (1991).
26. Samuels, A., Perry, M. J. & Tobias, J. H. High-Dose Estrogen Induces De Novo Medullary Bone Formation in Female Mice. *J. Bone Miner. Res.* **14**, 178–186 (1999).
27. Arai, N. et al. Expression of bone sialoprotein mRNA during bone formation and resorption induced by colchicine in rat tibial bone marrow cavity. *J. Bone Miner. Res.* **10**, 1209–1217 (2009).
28. Caselli, G., Fiorentino, S., Riminucci, M., Corsi, A. & Bianco, P. Does Colchicine really induce bone formation in the rodent bone marrow? Yes, it Does. *Calcif. Tissue Int.* **65**, 414–415 (1999).
29. Sivaraj, K. K. et al. Regional specialization and fate specification of bone stromal cells in skeletal development. *Cell Rep.* **36**, 109352 (2021).
30. Grüneboom, A. et al. A network of trans-cortical capillaries as mainstay for blood circulation in long bones. *Nat. Metab.* **1**, 236–250 (2019).
31. Riminucci, M., Saggio, I., Gehron Robey, P. & Bianco, P. Fibrous dysplasia as a stem cell disease. *J. Bone Miner. Res.* **21**, 125–131 (2006).
32. Piersanti, S. et al. Transfer, analysis and reversion of the fibrous dysplasia cellular phenotype in human skeletal progenitors. *J. Bone Miner. Res.* **25**, 1103–1116 (2009).
33. Kusumbe, A. P., Ramasamy, S. K., Starsichova, A. & Adams, R. H. Sample preparation for high-resolution 3D confocal imaging of mouse skeletal tissue. *Nat. Protoc.* **10**, 1904–1914 (2015).
34. Dempster, D. W. et al. Standardized nomenclature, symbols, and units for bone histomorphometry: A 2012 update of the report of the ASBMR Histomorphometry Nomenclature Committee. *J. Bone Miner. Res.* **28**, 2–17 (2013).
35. Tratwal, J. et al. Reporting Guidelines, Review of Methodological Standards, and Challenges Toward Harmonization in Bone Marrow Adiposity Research. Report of the Methodologies Working Group of the International Bone Marrow Adiposity Society. *Front. Endocrinol. (Lausanne)* **11**, 65 (2020).
36. Bravenboer, N. et al. Standardised Nomenclature, Abbreviations, and Units for the Study of Bone Marrow Adiposity: Report of the Nomenclature Working Group of the International Bone Marrow Adiposity Society. *Front. Endocrinol. (Lausanne)* **10**, 923 (2020).
37. Schneider, C. A., Rasband, W. S. & Eliceiri, K. W. NIH Image to ImageJ: 25 years of image analysis. *Nat. Methods* **9**, 671–675 (2012).
38. Robey, P. G., Kuznetsov, S. A., Riminucci, M. & Bianco, P. Bone marrow stromal cell assays: In vitro and in vivo. *Methods Mol. Biol.* **1130**, 279–293 (2014).
39. Rostovskaya, M. et al. Clonal analysis delineates transcriptional programs of osteogenic and adipogenic lineages of adult mouse skeletal progenitors. *Stem Cell Rep.* **11**, 212–227 (2018).
40. Gordon, M. N., Osterburg, H. H., May, P. C. & Finch, C. E. Effective oral administration of 17β-Estradiol to female C57BL/6J mice through the drinking water. *Biol. Reprod.* **35**, 1088–1095 (1986).